

Star clusters of the Andromeda galaxy. Multicolour HST photometry

Rokas Naujalis¹ , Rima Stonkutė^{1,2} and Vladas Vansevičius^{1,2}

¹Center for Physical Sciences and Technology, Saulėtekio av. 3, 10257 Vilnius, Lithuania
email: rokas.naujalis@ftmc.lt

²Vilnius University Observatory, Čiurlionio 29, 03100 Vilnius, Lithuania
email: vladas.vansevicius@ff.vu.lt

Abstract. We performed a new integrated photometry in six passbands on HST M31 PHAT survey mosaics of 1181 star clusters spread over a large range of radial distance. Due to strongly varying background we interactively determined its level based on image and growth-curve analysis. We derived cluster age, mass, extinction, and metallicity by employing stochastic star cluster models.

Keywords. galaxies: individual: M 31, galaxies: star clusters: general

1. Introduction

Star cluster studies can provide a wealth of information about star formation processes inside galaxies. Various analysis methods exist for parameter determination of semi-resolved clusters: colour-magnitude diagram of individual cluster stars ([Johnson et al. 2016](#)), integrated spectroscopy ([Caldwell et al. 2009, 2011](#)), and integrated photometry ([Fouesneau & Lançon 2010; de Meulenaer et al. 2013](#)). We use the integrated photometry method because it allows to study fainter star clusters.

The Hubble Space Telescope (HST) Panchromatic Hubble Andromeda Treasury (PHAT, [Dalcanton et al. 2012](#)) survey provides unprecedented photometric depth and angular resolution. It covers a large part of the M31 disk from the center to the outskirts. High angular resolution provides means to reliably identify and study even low mass star clusters. We use a star cluster sample from [de Meulenaer et al. \(2017\)](#) which is a subsample of clusters published by [Johnson et al. \(2015\)](#). Six photometric passbands covering a large wavelength range from $0.26 \mu\text{m}$ up to $1.7 \mu\text{m}$ are essential in disentangling star cluster parameter degeneracies.

2. Aperture photometry

The PHAT survey is divided into 23 regions called ‘bricks’. We omitted the 4 ‘bricks’ closer to the M31 center in order to avoid the extremely high density of stellar background which significantly reduce the reliability of photometric measurements. This left us with a sample of 1181 star clusters. An example of the cluster imaging data used for the analysis is shown in Fig. 1.

A large diversity of cluster morphology and background crowding make it difficult to apply automated photometry methods. Therefore, we performed star cluster photometry by interactively adjusting cluster center positions, determining background levels, and selecting aperture sizes (R_C & R_M , see Fig. 1). We measured growth-curves of each cluster in all six passbands up to 5 arcsec. Areas beyond the applied apertures were used to evaluate the local background level. We developed a custom user interface to

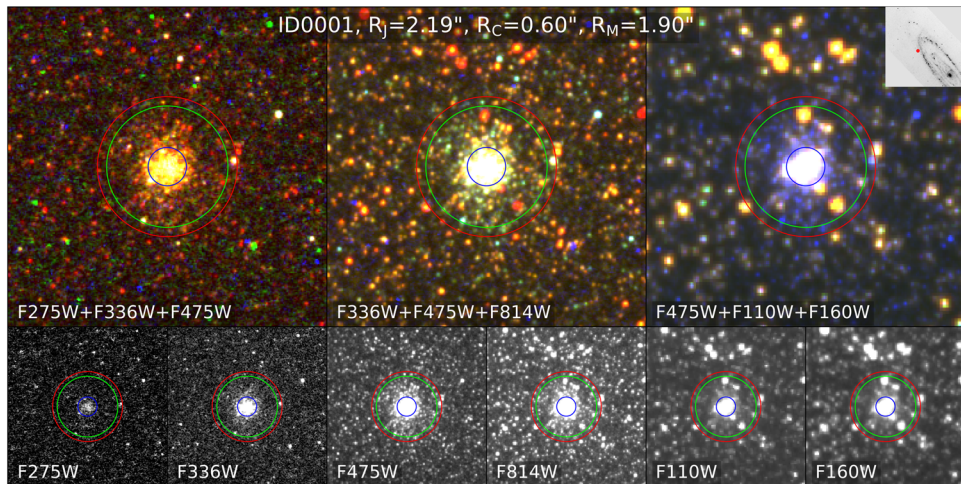


Figure 1. Images of the cluster ID0001 in all 6 PHAT passbands (bottom row) and colour combinations (top row). The apertures used for photometry are marked by colour circles: red – used by (Johnson *et al.* 2015, R_J); blue – used to determine the cluster colours (R_C); green – used to determine of the cluster total magnitude in the $F475W$ passband (R_M).

interactively estimate the sky background level based on a visual inspection of multi-colour cluster images, the growth-curves and their differential profiles. This allowed us to determine consistently the background level in all six passbands by rejecting bright foreground/background sources that would otherwise severely affect photometry results.

We selected two apertures for each cluster (Fig. 1): a smaller one (R_C , blue circle) to derive cluster colours and a larger one (R_M , green circle) to derive the total cluster magnitude in the $F475W$ passband, because it has the best signal-to-noise ratio and it is relatively less contaminated by foreground/background stars, that often dominate in the infrared passbands. We determined total magnitudes and aperture corrections for the R_C aperture measurements in the $F475W$ passband. We used significantly smaller apertures, compared to the cluster sizes, for colour measurement; therefore, we assume the absence of a radial colour gradient within a cluster. Finally, we applied aperture corrections in each passband to the magnitudes measured in the R_C aperture.

Comparisons of photometric magnitudes (Fig. 2) and colours (Fig. 3) measured in this study and by Johnson *et al.* (2015) show large differences, especially in the UV and IR passbands. These results suggest performing a careful interactive analysis of the semi-resolved clusters and their surroundings in order to obtain correct photometric measurements of clusters which have a very different morphology and reside on uneven sky backgrounds.

3. Star cluster parameters

We derive star cluster parameters (age, mass, extinction, and metallicity) by comparing cluster integrated magnitudes to the synthetic star cluster grid (Fouesneau & Lançon 2010, de Meulenaer *et al.* 2017 and references therein). The grid is filled with the cluster models that cover the ranges: age from $\log_{10}(t/\text{yr}) = 6.6$ to 10.1 in steps of 0.05; mass from $\log_{10}(\text{M}/\text{M}_\odot) = 2$ to 6 in steps of 0.05; and metallicity from $[\text{M}/\text{H}] = -2.2$ to +0.4 in steps of 0.2. To account for stochasticity effects, we calculate 1000 cluster models at each node with a random sampling of the initial mass function (Kroupa 2001) following the method described in Deveikis *et al.* (2008). We use the PARSEC isochrones

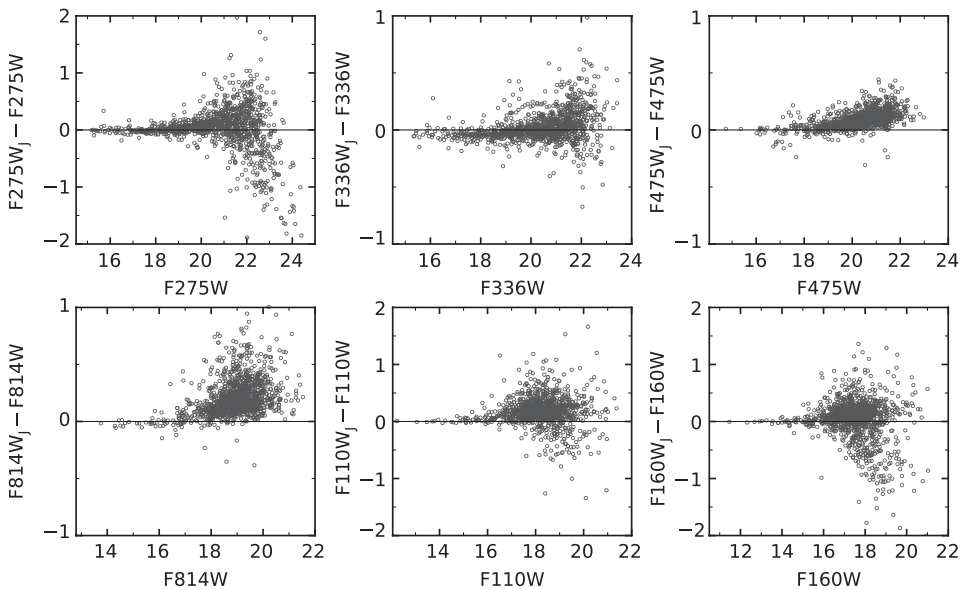


Figure 2. Magnitude differences of cluster photometry, published by Johnson *et al.* (2015) (marked with index ‘J’) and measured in this study, plotted versus corresponding magnitudes.

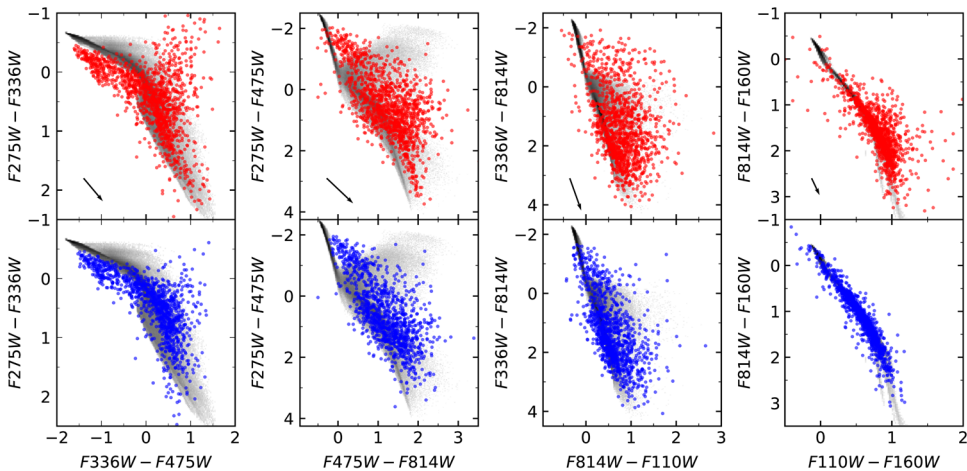


Figure 3. Colour-colour plots of the 1181 clusters studied. Photometry results are from Johnson *et al.* (2015) (red dots, upper panels) and measured in this study (blue dots, bottom panels). Gray-shaded regions show the spread of synthetic star clusters with a mass equal to $1000 M_{\odot}$. Extinction vectors correspond to $A_V = 1$ mag.

by Bressan *et al.* (2012). To optimise the required computer memory, the extinction is computed during the comparison of observations with the grid of models. Extinction values range from $E(B-V) = -0.03$ to 1.00 in steps of 0.01. Foreground Milky Way extinction was set to $E(B-V) = 0.055$ with $R_V = 3.1$. We calculated the likelihood of each node of the grid to represent the observed magnitudes as described in detail by de Meulenaer *et al.* (2013, 2014, 2015).

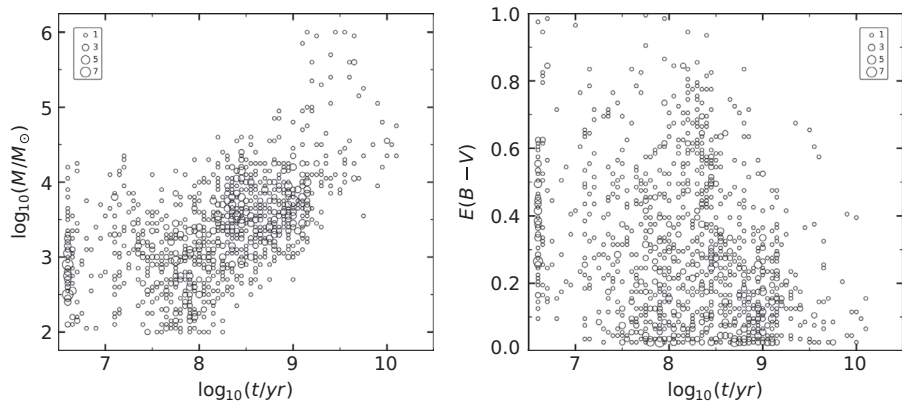


Figure 4. Parameters derived for 1181 clusters: mass versus age (left panel) and extinction versus age (right panel). Symbol sizes code the number of clusters overlapping at each point of the diagrams.

4. Discussion

Derived cluster mass and extinction values versus age are shown in Fig. 4. A clear pattern of mass versus age is visible and it is caused by two factors: a quicker disruption of lower mass clusters from galactic tidal forces as well as fading magnitudes of older clusters which make them much harder to detect.

The most massive globular-like cluster ages vary from ~ 2 Gyr to 12 Gyr, which on average indicate younger ages than in the Milky Way. However, this feature could have arisen artificially due to the applied upper limit of the model cluster mass of $10^6 M_\odot$.

Extinction values of clusters vary depending on their location with respect to the M31 galaxy disk: in front of or behind interstellar clouds that are concentrated on the disk plane. However, we should note that the extinction determination procedure is very sensitive to projected foreground/background objects.

The youngest clusters of an age of 4–6 Myr seem to have on average larger extinction values, which may indicate that they are still surrounded by interstellar clouds in the native star-forming regions. However, the youngest clusters are also often part of larger stellar associations and their individual parameters are not very reliable.

References

- Bressan, A., Marigo, P., Girardi, L., et al. 2012, *MNRAS*, 427, 127
- Caldwell, N., Harding, P., Morrison, H., et al. 2009, *AJ*, 137, 94
- Caldwell, N., Schiavon, R., Morrison, H., et al. 2011, *AJ*, 141, 61
- Dalcanton, J. J., Williams, B. F., Lang, D., et al. 2012, *ApJS*, 200, 18
- de Meulenaer, P., Narbutis, D., Mineikis, T., & Vansevičius, V. 2013, *A&A*, 550, A20
- de Meulenaer, P., Narbutis, D., Mineikis, T., & Vansevičius, V. 2014, *A&A*, 569, A4
- de Meulenaer, P., Narbutis, D., Mineikis, T., & Vansevičius, V. 2015, *A&A*, 574, A66
- de Meulenaer, P., Stonkutė, R., & Vansevičius, V. 2017, *A&A*, 602, A112
- Deveikis, V., Narbutis, D., Stonkutė, R., et al. 2008, *BaltA*, 17, 351
- Fouesneau, M. & Lançon, A. 2010, *A&A*, 521, A22
- Johnson, L. C., Seth, A. C., Dalcanton, J. J., et al. 2015, *ApJ*, 802, 127
- Johnson, L. C., Seth, A. C., Dalcanton, J. J., et al. 2016, *ApJ*, 827, 33
- Kroupa, P. 2001, *MNRAS*, 322, 231